Langmuir

Article

pubs.acs.org/Langmuir

Inhibition of Antithrombin and Bovine Serum Albumin Native State Aggregation by Heparin

Burcu Baykal Minsky, Bingqian Zheng, and Paul L. Dubin*

Department of Chemistry, University of Massachusetts, Amherst, Massachusetts, 01003, United States

ABSTRACT: Protein native state aggregation, a major problem in pharmaceutical and biological processes, has been addressed pharmacologically by the addition of protein-binding excipients. Heparin (Hp), a highly sulfated polysaccharide, interacts with numerous proteins with moderate to high affinity, but reports about its effect on protein aggregation are contradictory. We studied the pH dependence of the aggregation of antithrombin (AT) and bovine serum albumin (BSA) in the presence and absence of heparin. High-precision turbidimetry showed strong aggregation for both AT and BSA in I = 10 mM NaCl, conditions at which electrostatically driven Hp binding and aggregation both occur, with more obvious aggregation of heparin-free AT appearing as larger aggregate size. Aggregation of AT was dramatically inhibited at Hp:protein 6:1 (mole ratio); however, the effect at 0.5:1 Hp:protein was greater for BSA. Frontal analysis capillary electrophoresis showed a much larger equilibrium association constant K_{obs} between Hp and AT, in accord with the onset of Hp binding at a higher pH; both effects are explained by the higher charge density of the positive domain for AT as revealed by modeling with DelPhi. The corresponding modeling images showed that these domains persist at high salt only for AT, consistent with the 160-fold drop in K_{obs} at 100 mM salt for BSA−Hp binding. The smaller inhibition effect for AT arises from the tendency of its uncomplexed monomer to form larger aggregates more rapidly, but the stronger binding of Hp to AT does not facilitate Hp-induced aggregate dissolution which occurs more readily for BSA. This can be attributed to the higher density of AT aggregates evidenced by higher fractal dimensions. Differences between inhibition and reversal by Hp arise because the former may depend on the stage at which Hp enters the aggregation process and the latter on aggregate size and morphology.

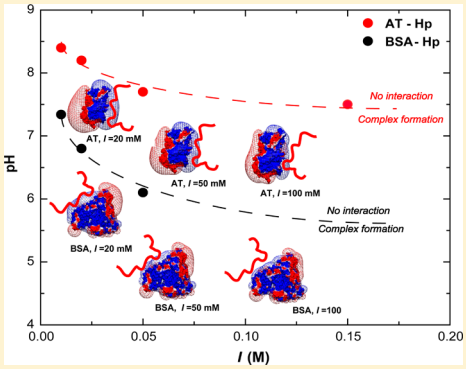

INTRODUCTION

The effect of heparin (Hp) on protein aggregation would appear from the literature to comprise both promotion and inhibition. These conflicting results could reflect the problem of comparing different proteins with different levels of Hp affinity and different aggregation mechanisms, both dependent on solution pH and ionic strength. Native state aggregation could facilitate formation and interpretation of Hp effects, because protein surface is better conserved and formation of unfolded states minimized. Native state protein aggregation is driven by electrostatics, and the protein surface charge anisotropy regulates protein self-association mechanisms. Electrostatics also controls Hp−protein binding. There is a need to explain the possible linkage between electrostatically driven native state aggregation and Hp−protein binding. It is of interest to establish whether this relation holds for "heparin-binding" proteins which exhibit different Hp affinities, such as antithrombin (AT) and bovine serum albumin (BSA). Therefore, we studied the native state aggregation of AT and BSA and the roles of Hp in both aggregation and disaggregation processes, using ionic strength (I) and pH as probes to investigate protein self-association mechanisms and Hp binding affinities.

The detection of GAGs in deposits of fibrillar aggregates in amyloid diseases initiated a number of conflicting hypotheses about the promotion/inhibition of the aggregation of amyloid-forming peptides and proteins in the presence of GAGs. The enhancement of gelosin aggregation by heparin (Hp) was correlated with its sulfate content and MW.[1] Both Hp and CS (chondroitin sulfate) appeared to promote Aβ peptide aggregation.[2] On the other hand, while p25-α aggregated in the presence of stoichiometric amounts of low-MW Hp (10−14 monosaccharides), excess Hp diminished its aggregation.[3] Hp induces aggregation/fibril formation of some proteins under certain conditions but may have more ambiguous or even benign effects, depending on conditions, as observed for the prion protein.[4,5] Injection of low molecular weight heparin suppresses AA amyloid deposition in mice,[6] and even when fibrils are promoted by Hp they are less toxic than the earlier forms of aggregates.[2,7−9] Finally, inhibition of Aβ aggregation is reported for GAG-mimetic sulfated glycopolymers.[10]

These conflicting reports of Hp effects on amyloidogenesis may arise because the point at which Hp enters the aggregation process can vary and is often not well-defined. This suggests that effects of Hp could be better understood with systematic studies with folded proteins that include elucidation of self-aggregation mechanisms and identification of the aggregation stage influenced by Hp. The self-aggregation of folded proteins

Received: October 10, 2013
Revised: December 6, 2013
Published: December 8, 2013

is mostly studied under "accelerated" conditions, such as high temperature[11] and low pH;[12−15] these conditions, however, generally lead, either intentionally or fortuitously, to formation of intermediate states of the native structure, and the contribution of these states to the aggregation processes could be difficult to evaluate.[16] The two proteins chosen for study here, AT and BSA, are examples of this as both of them are commonly studied at elevated temperatures.[17−21] In contrast, the influence of Hp on native state aggregation can be more amenable to modeling,[22] and therefore, consistent with general rules; the hydrated protein surface is retained, and formation of intermediate states can be minimized. The charge distribution on this surface, which plays a central role in interprotein interactions,[23,24] is controlled by protein structure and pH.

Although native state protein aggregation is most readily seen at pH ∼ pI ("isolectric precipitation"), its suppression by added salt indicates the primacy of electrostatic attraction.[25] The central role of interprotein surface interactions makes such aggregation amenable to colloid models, in which the aggregation kinetics could determine the aggregate structure. Aggregation follows formation of clusters from monomers, and growth could follow particle−cluster or cluster−cluster, and formation of these could be limited by diffusion.[26] As shown in previous work,[22,25] protein charge anisotropy dictates the balance of attractive and repulsive electrostatic interactions that leads to one or more of the preceding aggregation mechanisms, which then control aggregate structure. The charge anisotropy of proteins also controls their interactions with Hp,[27] and this suggests an implicit linkage between heparin suppression and electrostatic aggregation.[22,25] For example, Hp inhibits native state aggregation of BSA and BLG, with the inhibitory effect depending on charge-induced Hp−protein binding affinity.[22] Beyond affinity, the stage at which Hp enters the aggregation process plays an important role: inhibition of the aggregation of native state insulin seems to be enhanced when Hp is added after aggregation has begun.[25] The availability of Hp-binding domains is evidently subject to alterations in protein conformation.[28] In the present work, we avoid contributions of protein unfolding by selection of conditions and by focusing on two stable proteins, AT and BSA.

Heparin−protein binding affinity arises principally from polyelectrolyte−protein electrostatic interactions,[29,30] for which different models have been widely applied. One model, inspired by theories for the salt dependence of oligolysine−DNA interactions[31,32] has also been applied to DNA−protein binding. The linear dependence of log K_{obs} (equilibrium association constant) on log I (ionic strength) is consistent with a purely entropic ΔG_{obs} which arises from the release of DNA counterions. However, directly replacing oligolysines with proteins fails to consider the influence of protein charge anisotropy.[33] Nevertheless, extension of this treatment to Hp−protein binding yields a physically realistic value of Hp structural charge density deduced from measured dlog K_{obs}/dlog I.[34] On the other hand, many polyelectrolyte−protein systems show clearly different salt dependence, more consistent with Debye−Hückel screening.[29,35] This model takes into account protein charge anisotropy and effectively explains the nonmonotonic salt dependence seen when polyelectrolytes (e.g., heparin) bind to proteins with net charge of the same (i.e., negative) sign, through a domain of opposite (i.e., positive) charge. This domains is best identified through representation of protein charge calculations.[36] Therefore, it is possible to account for the observed salt dependence of protein−Hp binding by using specific models of heparin binding along with quantitative protein visualization.[36,37]

The way in which Hp inhibits protein aggregation depends on Hp−protein binding affinity and the stage at which Hp enters the aggregation process. The ability of Hp to reverse aggregation depends also on aggregate structure. Resolution among these effects has not been achieved because variables such as pH and ionic strength, influence both the mechanism and rate of aggregation and the interaction of Hp with either aggregates or free proteins. Protein charge anisotropy could in fact enhance both interprotein and Hp−protein interactions. Systematic studies of pH and ionic strength effects on appropriately selected aggregating and heparin-binding proteins are needed to elucidate these primarily electrostatic effects. Also further insight into the effect of heparin on protein solubility could help guide the extensive but largely empirical use of polyelectrolyte precipitation for protein purification.[38−40]

In order to elucidate the way in which the antiaggregation effect of Hp is influenced by protein self-association and Hp affinity, we examine two Hp-binding proteins, Hp cognate AT and noncognate BSA. The literature clearly indicates larger rates of aggregation for AT than for BSA,[18] although their mechanisms of aggregation differ.[18,41] In our work, native states have been preserved; so therefore, the behavior of the proteins is determined by its (hydrated) surface. For this reason, general rules about aggregation (e.g., "isoelectric precipitation") can be put forward, in contrast to unfolding aggregation in which any or all residues may contribute to a wide variety of interactions involving many intermediates. We used high-precision turbidimetry to assess both aggregation rates and Hp affinity and dynamic light scattering (DLS) to determine the size and the relative intensity of the aggregates as a function of pH and ionic strength. The fractal dimensions of the respective aggregates were measured by static light scattering. Electrostatic protein modeling was used to visualize domains of positive charge and to rationalize both aggregation and Hp binding.

Experimental Section. *Materials.* Human recombinant AT (ATyrn, 58 kDa, pI ∼ 5.0) was generously donated by GTC Biotherapeutics (Framingham, MA). Bovine serum albumin (BSA, 66 kDa, pI ∼ 4.9) and heparin (Hp), with nominal MW 14 kDa, were purchased from Calbiochem and Sigma, respectively.

Methods. Turbidimetry. High-precision turbidimetry was performed using a Brinkman PC800 digital display probe colorimeter equipped with a 1 cm path length probe (at 420 nm), integrated into a system of our own design which is programmed for (1) automated constant delivery of selected titrant volume at selected rates of addition via a 2 mL Gilmont microburet, (2) the number of transmittance (%T) and pH readings to be averaged, and (3) choice of the terminal pH. AT (0.25 g/L, 10 mL total volume) and BSA (1g/L, 10 mL total volume) solutions were prepared at desired NaCl concentrations (10−50 mM), filtered (0.22 μm Millipore), and titrated with either 0.1 N HCl or 0.1 N NaOH. AT−Hp and BSA−Hp mixtures were prepared by 1:1 v/v mixing of AT/BSA and Hp stock solutions (0.5 g/L) at a noninteracting pH 8.5 (±0.2). All measurements were done at ambient temperature. The precision in the volume of titrant added is typically ±2 ppt (0.2%). The ability to average multiple readings leads to transmittance measurement with a precision of 0.1 %T (±1 ppt).

dx.doi.org/10.1021/la4039232 | *Langmuir* 2014, 30, 278−287

Dynamic Light Scattering (DLS). DLS measurements were made after filtration (Millipore 0.22 μm) using a Malvern Instruments Zetasizer Nanosystem ZS, with a 633 nm He−Ne laser operating at 173° scattering angle, at 25 °C. The measurement duration was 10−12 s. The distributions of the mean apparent translational diffusion coefficients (D_T) were determined by fitting the DLS autocorrelation functions using nonnegative constrained least-squares (NNLS). The distribution of apparent hydrodynamic diameters D_h was obtained from the distribution of mean apparent translational diffusion coefficients (D_T) via

$$D_h = \frac{2kT}{6\pi\eta D_T} \quad (1)$$

where k is the Boltzmann constant and η is the solvent viscosity, taken as that of water. Sample transfer and automated optimization steps result in a delay of 2−3 min between initial pH adjustment and the first measurement.

Static Light Scattering (SLS). SLS experiments were performed using a BI-200 SM goniometer and BIC-2030D photon-counting system (Brookhaven Instruments Inc.) with an Omnichrome Ar ion laser (100 mW, λ = 488 nm) at ambient temperature, 25 °C. The scattering intensity was measured as a function of scattering angle between 45 and 130°. Fractal dimensions (D_f) were extracted from angle dependence in the high-q limit via linearization of the scattering data using the relation

$$I(q) \propto q^{-Df} \quad (2)$$

where $I(q)$ is the scattering intensity and the scattering vector $q = (4\pi n/\lambda)\sin(\theta/2)$, with n the refractive index of the fluid, λ the wavelength, and θ the scattering angle. The radius of gyration (R_g) was obtained using Guinier relation at relatively low-q region:

$$\ln(I(q)) = \ln\left(I(0) - \frac{q^2 R_g^2}{3}\right) \quad (3)$$

Computational Methods. DelPhi V.4r1.1[42,43] was used to model the electrostatic potential around the protein as a function of ionic strength. PDB id is 3 V03 and 2B4X were taken from the Protein Data Bank (http://www.rcsb.org/) for BSA monomer and AT monomer, respectively. The charges of amino acids on the proteins were determined using the spherical-smeared charged model put forward by Tanford.[44]

RESULTS

Protein Aggregation: Effects of pH. *AT Shows Higher Turbidimetric Rates of Aggregation.* Figure 1 shows the increase in 100 − %T in the range 4 < pH < 7 upon addition of acid to 1 g/L BSA in 10 mM NaCl. A reduced concentration of 0.25 g/L was used for the more rapidly aggregating AT in order to maintain 100 − %T < 20. In this range 100 − %T is linear with the true turbidity τ = −log T and can be most readily identified with the accumulation of soluble aggregates.[45,46] The pH for the onset of aggregation is qualitatively seen to be about 1 pH unit above pI for AT, in contrast to BSA for which pI − pH = 0.5. Since protein concentrations are not the same, the difference in absolute values of τ is handled by comparing the turbidimetric rates of aggregation $(d\tau/dt)_{pH}$. This is calculated as $(d\tau/dpH)\,(dpH/dt)$, where $(d\tau/dpH)$ is obtained from Figure 1, and dpH/dt is automatically recorded at every pH. In the resultant plot (inset of Figure 1), $(d\tau/dt)_{pH} = 0$ would correspond to a maximum. This indicates equal turbidimetric rates of aggregation and disaggregation.[46,47] The maximum rate of aggregation $(d\tau/dt)_{pH}^{max}$ is seen at pH 6 and 5.5 for AT and BSA, respectively. For BSA, the native state is preserved over a wide range of pH encompassing the experimental conditions here.[48−50] For AT, there are additional suggestions of partial unfolding,[51] but not at pH ∼ 6 as used here. Those studies refer to the dynamics of loop expulsion, presumably at a time scale that is not relevant to our measurements of relatively slow aggregation.

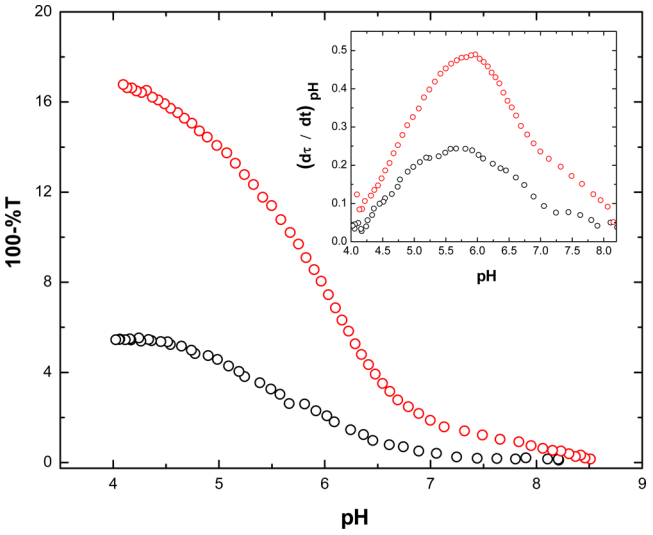

Figure 1. Automated turbidimetric titrations of 0.25 g/L AT (red) and 1 g/L BSA (black) in 10 mM NaCl with the addition of 0.1 N HCl. Inset: Aggregation rate (dτ/dt) vs pH obtained from Figure 1 for AT (red) and BSA (black).

Time Dependence of AT and BSA Aggregation Can Reveal Aggregation Mechanisms. Figure 2 shows time-dependent turbidities for AT and BSA under concentration and ionic

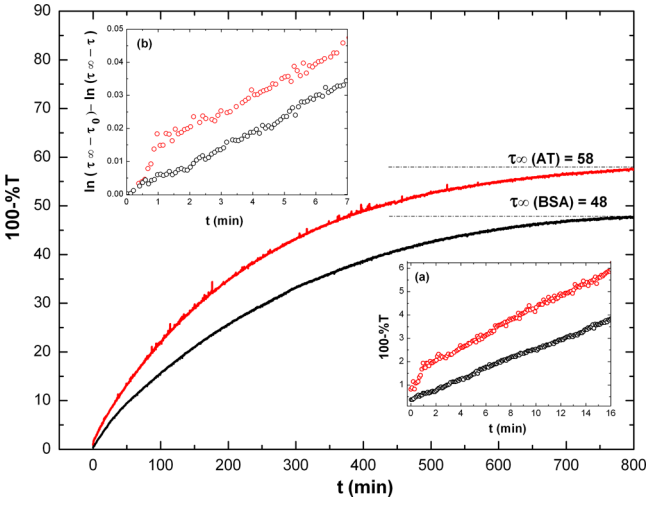

Figure 2. Turbidimetric measurements in 10 mM NaCl for the time-dependent aggregation of 0.25 g/L AT at pH 6.1 (red) and 1 g/L BSA at pH 5.4 (black). Samples were prepared at high pH (∼8.5) and then brought to the desired pH within 3 min using 0.1 N HCl. Inset (a): Expanded time scale for the first 16 min. Inset (b): First-order fit for the time vs τ (100 − %T) for AT (red) and BSA (black) in the first 7 min.

dx.doi.org/10.1021/la4039232 | *Langmuir* 2014, 30, 278−287

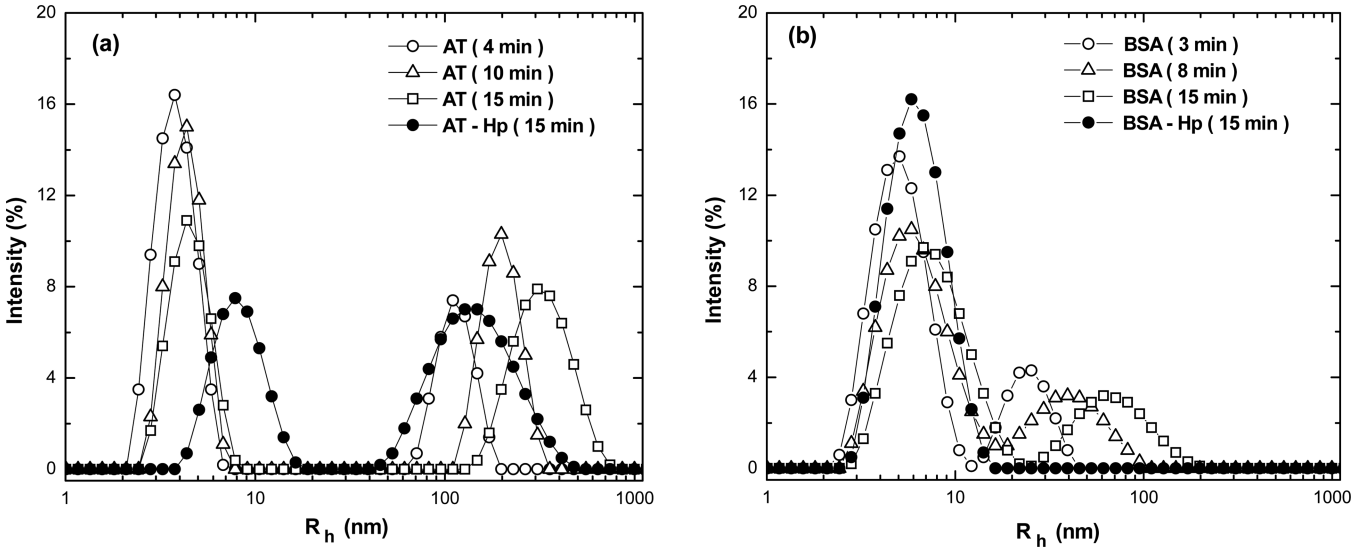

Figure 3. Time dependence of particle sizes by DLS in 10 mM NaCl in the absence and presence of Hp: (a) 1 g/L AT and 1 g/L AT with 0.1 g/L Hp (●) at pH 6.2; (b) 1 g/L BSA and 1 g/L BSA with 0.1 g/L Hp (●) at 5.4.

strength and pH conditions in the vicinity $(d\tau/dt)_{pH}^{max}$ in Figure 1. Since $c_{AT}/c_{BSA} = 0.25$, we focus on mechanistic differences, which are independent of protein concentration. In Figure 2, the turbidity reaches a limiting value for AT and BSA at similar times, with a larger limiting value for the former. The turbidity of AT increases rapidly for $t < 1.5$ min (Figure 2, inset a), while the curve for BSA exhibits only a small decrease in curvature at $t = 25$ min. Figure 2, inset b compares the aggregation kinetics of AT and BSA using first-order plots obtained from the data in Figure 2. The analysis of turbidity data can be described as[52,53]

$$\tau = \tau_\infty(1 - e^{-kt}) \quad (4)$$

where τ_∞ is the limiting turbidity value at $t = \infty$, and k is the apparent rate constant. The first-order appearance of the aggregation kinetics may indicate the mechanisms of aggregation for both proteins (vide infra). The evolution of aggregates was also probed with DLS (Figure 3) in the absence and presence of Hp (the latter will be explained below). Contrary to turbidimetry, DLS cannot capture the first 2 min due to the time lag between the sample pH adjustment and measurement but provides a better molecular view, as seen in Figure 3a, in which $c_{AT} = c_{BSA} = 1$ g/L. The experimental lag time notwithstanding, the rapid increase in turbidity for AT can be related to the increase in cluster size, from <100 to 300 nm during the first 15 min. Two differences appear in Figure 3b for BSA: the fast mode broadens as opposed to losing intensity, and the slow-mode size increases by only a factor of 2.5, from 25 to 65 nm. The larger apparent initial rate from turbidity for AT appears to be due to rapid increase in aggregate size (Figure 3a) at the end of which the fast mode (monomer) no longer dominates the scattering intensity (data not shown).

Effect of Heparin on Protein Aggregation. *Heparin Suppresses Aggregation of Both Proteins.* Figure 4 shows inhibition of AT and BSA aggregation in the presence of Hp at various Hp:protein (r) ratios. The inhibition of aggregation by Hp can be observed only in the "pH window" bounded by formation of the heparin–protein complexes. At $r = 0.1$, the stoichiometry best suited for comparison of BSA and AT, the suppression of the aggregation is more pronounced for BSA.

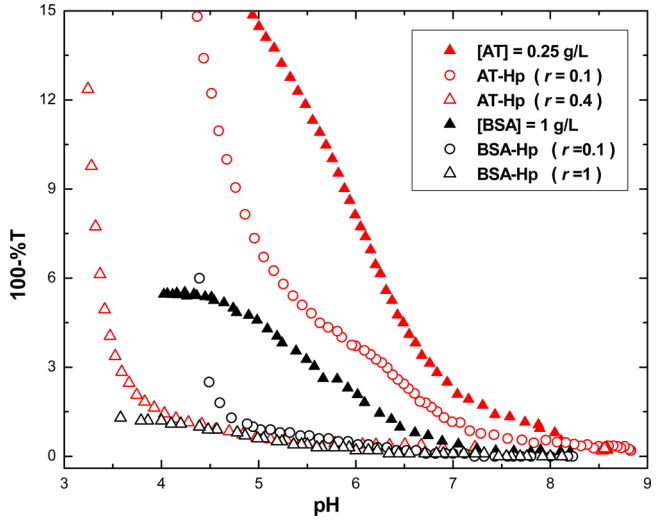

Figure 4. Inhibition of 0.25 g/L AT and 1 g/L BSA aggregation by heparin at 10 mM NaCl. Heparin to AT weight ratio (r) is 0.1 and 0.4 and heparin to BSA weight ratio (r) is 0.1 and 1.

This is confirmed by DLS results (Figure 3), in which data in the absence of Hp are combined with results in the presence of Hp approximately 15 min after pH adjustment (this time lag leads to a small increase in R_h for the slow mode for AT alone and to an increase in fast mode R_h for BSA alone). Here, we see that the fast-mode intensity of the free monomer (or in the case of BSA, monomer–dimer) never exceeds 50% for AT but the fast mode is always the dominant scatterer for BSA. A separate but related effect is the concentration of monomer or monomer/dimer in the presence of Hp, obviously dependent on both the Hp–protein binding affinity and the Hp:protein ratio r. At $r = 0.1$, the doubling of the apparent size corresponding to the fast mode for AT can only be explained by the conversion of AT monomer to its complex with Hp. In contrast, the fast mode for BSA at $r = 0.1$ consistently exhibits an apparent size equal to that of the BSA dimer, regardless of time; BSA–Hp complexes and possibly BSA dimers coexist at that condition.

dx.doi.org/10.1021/la4039232 | Langmuir 2014, 30, 278–287

AT–Hp Binding Less Sensitive to Salt. In order to evaluate the AT–BSA binding strength, we investigated the effect of salt concentration on the onset of Hp–protein complex formation (Figure 5). This event, pH_c experimentally defined by a

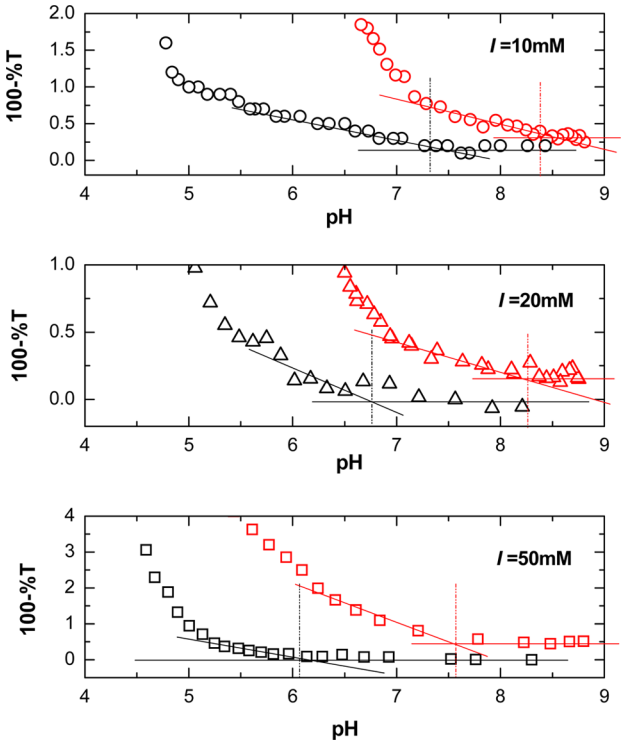

Figure 5. Turbidimetric titration of AT (red), BSA (black) (0.25 g/L), and Hp (0.025 g/L) at 10, 20, and 50 mM NaCl, using 0.1 N HCl. Red and black broken lines were used to indicate the pH_c values for AT and BSA, respectively.

transition from a region of zero slope reflects a reversible, equilibrium phenomenon as opposed to the purely or partially kinetic behavior described in all earlier figures. This critical pH qualitatively represents the condition at which the energy of complex formation just exceeds thermal energy, kT. When pH_c appears on the "wrong side of pI" (here when global protein charge is negative), $(pH_c - pI) = \delta pH$ becomes a qualitative measure of the ability of binding to overcome this global repulsion. Although AT and BSA have similar pI values (4.9 and 5.0), δpH is larger for AT at all ionic strengths. Addition of salt lowers δ for both AT and BSA, but the effect is more pronounced for BSA.

Hp Cannot Reverse AT Aggregation but Can Partially Reverse BSA Aggregation. The inhibition of AT and BSA aggregation in the presence of Hp is a result of soluble complex formation between protein and Hp. Hp may also interact with the larger aggregates dissolving them into small intrapolymer complexes[22,25] and in some cases larger interpolymer soluble species. Figure 6 shows the results for AT and BSA upon addition of Hp to a protein:Hp ratio $r = 1$ (w:w). The addition of Hp partially redissolves BSA aggregates (at pH 5.3) but does not reverse the aggregation of AT (at pH ~ 6.1).

DISCUSSION

AT and BSA Aggregation Mechanisms Are Different. The result for AT in Figure 2 inset b, which shows the first-order fit of turbidity vs time, is in agreement with nucleation (rapid initial consumption of monomer to form well-defined clusters) and growth (addition of monomer to these clusters), the first step difficult to observe for BSA. The initial AT cluster size could not be identified because of the time lag for DLS which can only identify after 4 min a 100 nm species for AT (Figure 3a) and a 25 nm species for BSA (Figure 3b). In the first 15 min, the rate of depletion of the AT monomer is slightly faster than that of the BSA monomer/dimer. There are two possible routes for the increase in turbidity over long times: clusters either grow by association ("cluster–cluster") or by adding monomer/dimer ("growth").[52] The first-order appearance of the curves in Figure 2 inset b for both proteins suggests that aggregates grow by the latter route. The transition from fast to slow steps, seen after 2 min for the aggregation of AT,

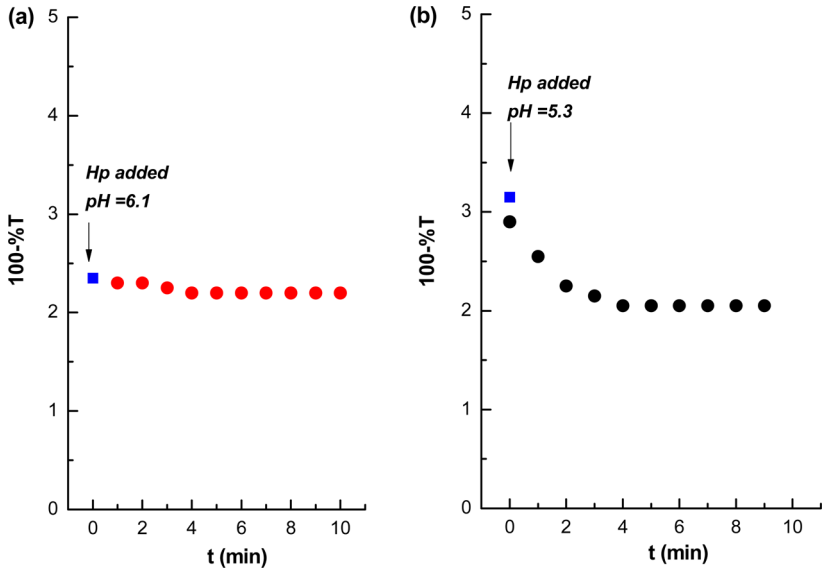

Figure 6. Reversal of aggregation in 10 mM NaCl: (a) 0.1 g/L AT and (b) 1 g/L BSA by the addition of Hp ($r = 1$). Both protein solutions were prepared at pH 8.5, and pH was adjusted to 6.1 for AT and 5.3 for BSA within 3 min using 0.1 N HCl. Solutions were kept for 20 min at room temperature prior to Hp addition.

dx.doi.org/10.1021/la4039232 | *Langmuir* 2014, 30, 278–287

Scheme 1. Models for the Aggregation Pathways of AT and BSA

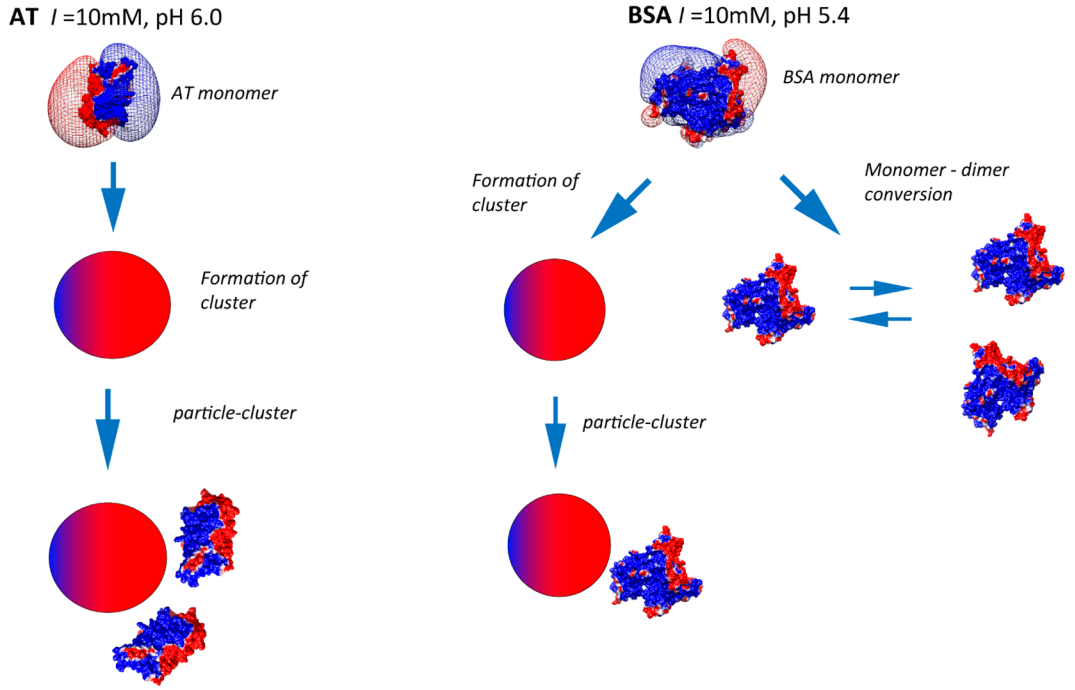

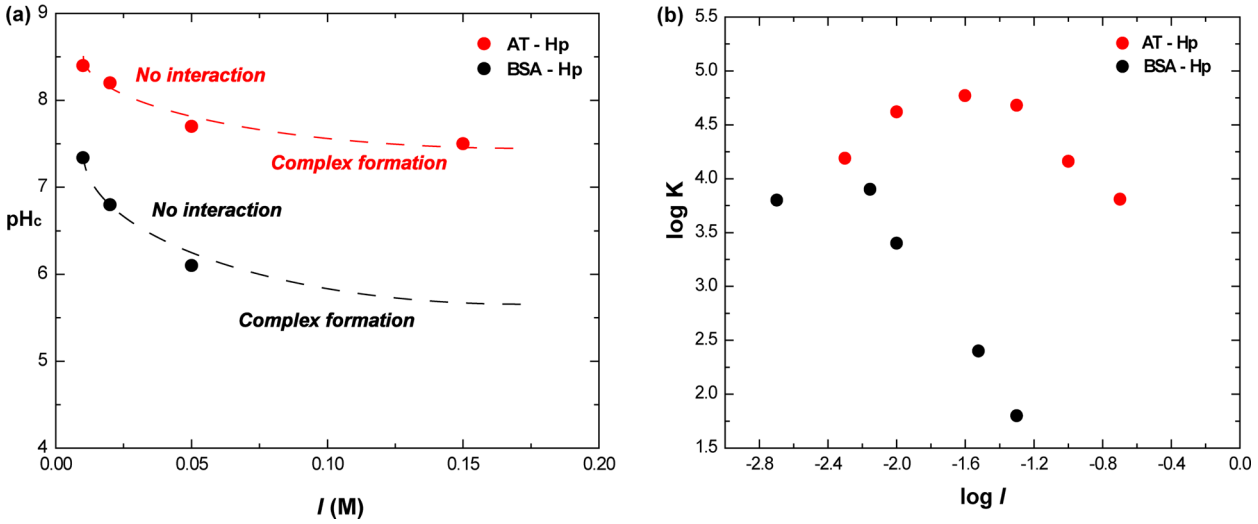

Figure 7. (a) Ionic strength dependence of pH_c obtained from turbidimetry (from Figure 5). The dashed lines are drawn to guide the eye. (b) Ionic strength dependence of the binding constant obtained by FACCE. The data for BSA and AT are from ref 36 and ref 37.

resembles that of BLG at pH near pI and in low salt. This protein also exhibits diffusion-limited particle−cluster aggregation as a second step.[47]

A notable difference between AT and BSA aggregation is seen in the evolution of the fast mode in Figure 3b for BSA, which in contrast to AT broadens and shifts to larger R_h with time. While R_h conforms to the AT monomer radius (4 nm) at all times, R_h increases from 5 to 8 nm for BSA in the interval 3−14 min, accompanied by peak broadening. We interpret these results as depletion of BSA monomer from the monomer−dimer pool, with the concentration of monomer then determining the rate of cluster growth, as opposed to cluster−cluster association. For AT, all unaggregated protein is present as the 4 nm monomer, and cluster growth is more rapid.

The absence of cluster−cluster association for both proteins can be explained by their net charge at pH − pI > 0. However, the interaction of negatively charged AT monomer with negatively charged clusters is ameliorated by the charge anisotropy of the AT monomer as depicted in Scheme 1. This same charge anisotropy also enhances monomer−monomer association kinetics and thus the rate of nucleation; this accounts for the nucleation step probably present for both protein but more readily detected for AT. Therefore, the greater charge anisotropy enhances the rate of nucleation.[46] The role of charge anisotropy of the BSA monomer is further complicated by its equilibrium with the dimer, as evidenced by the wide range of R_h values seen for its fast mode in Figure 3b. The increase from 5 to 7.5 nm during the first 10 min of aggregation can be best explained as the depletion of monomer

dx.doi.org/10.1021/la4039232 | Langmuir 2014, 30, 278−287

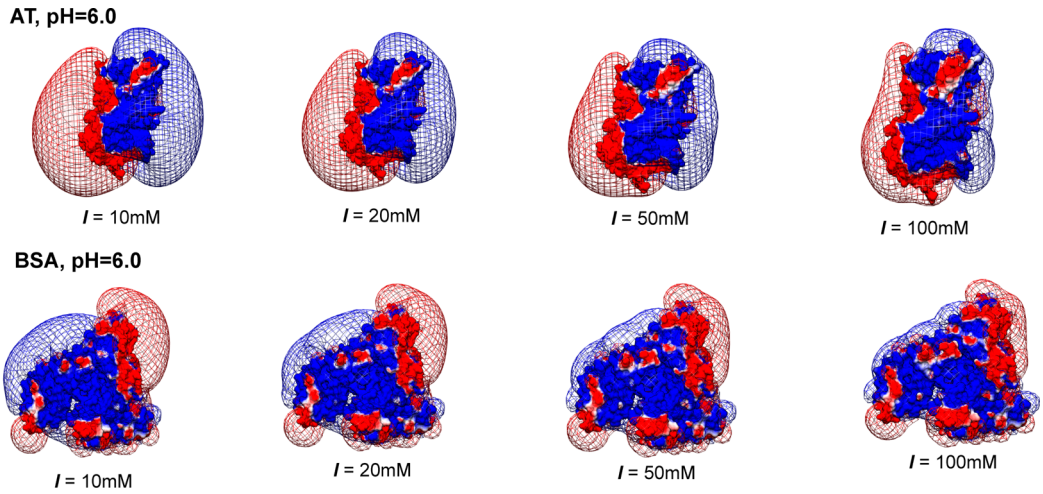

Figure 8. Ionic strength dependence of the electrostatic potential contours at −0.5 kT/e (red) and 0.5 kT/e (blue) for AT and BSA at pH 6.0.

through its preferential aggregation. In that sense, dissociation of dimer exerts some control over the rate of aggregation.

Inhibition of Aggregation Is a Result of Competition between Hp Binding and Self-Aggregation. The magnitude of heparin inhibition is qualitatively assessed by comparison of turbidimetric titrations with and without Hp for the two proteins. As shown in Figure 4, the inhibition effect depends on the heparin concentration (or bulk weight ratio r). Together with the protein−Hp binding affinity, this stoichiometry controls the fraction of protein that forms complex and thereby controls the aggregation rate by modulating the free protein concentration. The assumption is that heparin−protein complexes have no direct influence on aggregation kinetics. At r = 0.1, the concentration of total protein is fourfold smaller for AT than for BSA, but the intrinsically rapid aggregation of free AT results in larger turbidity.

Evidence of the depletion of protein monomer upon addition of Hp should emerge from DLS. In Figure 3a, AT monomer (R_h = 4 nm) is well resolved from complex at R_h = 8.5 nm and is seen to be fully converted to a mixture of small and large complexes in the presence of Hp. BSA aggregate clusters vanish in the presence of Hp (Figure 3b), but the ca. 8 nm complexes cannot be well resolved from BSA monomer/dimer. BSA monomer/dimer persists in the presence of Hp because of its relatively low Hp affinity, but BSA aggregates fail to form. The effect of Hp on BSA aggregation relative to its weaker effect on AT aggregation may be related to the differences in aggregate or aggregation mechanism, most notably the presence of an obvious nucleation step for AT. The amount of Hp required for suppression is r = 0.1 for BSA and r = 0.4 for AT. The larger requirement for AT suppression despite its stronger binding is a reflection of the strong tendency of its monomer to aggregate even at lower concentration. The second effect of r is the shift of pH_φ (phase separation pH) to lower pH.[22] This phase separation occurs when complexes achieve charge neutrality. When the ratio of Hp to protein is large, each Hp binds few proteins, and the positive charge per protein needed to overcome Hp charge is large, which corresponds to low pH_φ.

Stronger Binding of Hp to AT, Notably at High Salt, Manifested as High Values of pH_c. We proceed to interpret the results of Figure 5 in terms of binding constants for Hp−BSA and Hp−AT measured elsewhere. The ionic strength dependence of pH_c shown in Figure 7a provides a qualitative comparison of Hp affinity for AT vs BSA: the expanded domain of complexation seen for AT indicates its stronger heparin binding. Corresponding measurements by FACCE[36,37] verify this more quantitatively, and both measurements show that the difference in Hp affinity between AT and BSA strongly increases with added salt (Figure 7b). Interestingly, the frequently noted linear log−log dependence of Hp−protein binding[54] is seen to apply only at I > 10 mM for BSA and 25 mM for AT.

The differences between BSA and AT in Figure 7 can be explained by the charge distributions of the two proteins as represented by DelPhi images (Figure 8). The maximum in the plot for AT has been interpreted in terms of combined attractive and repulsive forces,[37] which should be more important for AT because of its charge anisotropy. The more pronounced positive domain for AT leads to the formation of an AT−Hp complex that is more salt resistant than the BSA−Hp complex. This is also reflected in the persistence at high salt of the positive (Hp-binding) electrostatic domain of AT and the virtual disappearance of this domain for BSA at 100 mM salt, entirely consistent with the drop in log K at log I = −1 for BSA in Figure 7b.

Aggregate Fractal Dimensions Larger for AT than for BSA. The greater charge anisotropy for AT vs BSA is not only consistent with its stronger Hp binding but may also explain the inability of Hp to reverse AT aggregation as shown in Figure 6. This apparently contradictory relation, the resistance to Hp-induced dissolution being greater for the protein with higher Hp affinity, can be understood in terms of aggregate formation and density. Recent Monte Carlo simulations have contrasted the aggregation behavior of uniformly and nonuniformly charged colloids, in which the latter interact more strongly and form larger clusters.[55] While both proteins here exhibit charge anisotropy, AT more nearly resembles the extreme case of nonuniform charge with correspondingly strong short-range attraction. This is expected to lead to a densely packed aggregate, resistant to dissolution. The binding of Hp as an inhibitor of aggregation can be considered energetically in terms of the equilibrium between complex and free protein, reducing its concentration and thus lowering the rate of aggregation. The stabilization of the former might be considered to arise from multiple interactions of the flexible Hp chain with the protein. Similar considerations have been referred to as "multivalency" but this does not reflect the role of polyelectrolyte chain dynamics. Aggregate *dissolution* follows a

dx.doi.org/10.1021/la4039232 | *Langmuir* 2014, 30, 278−287

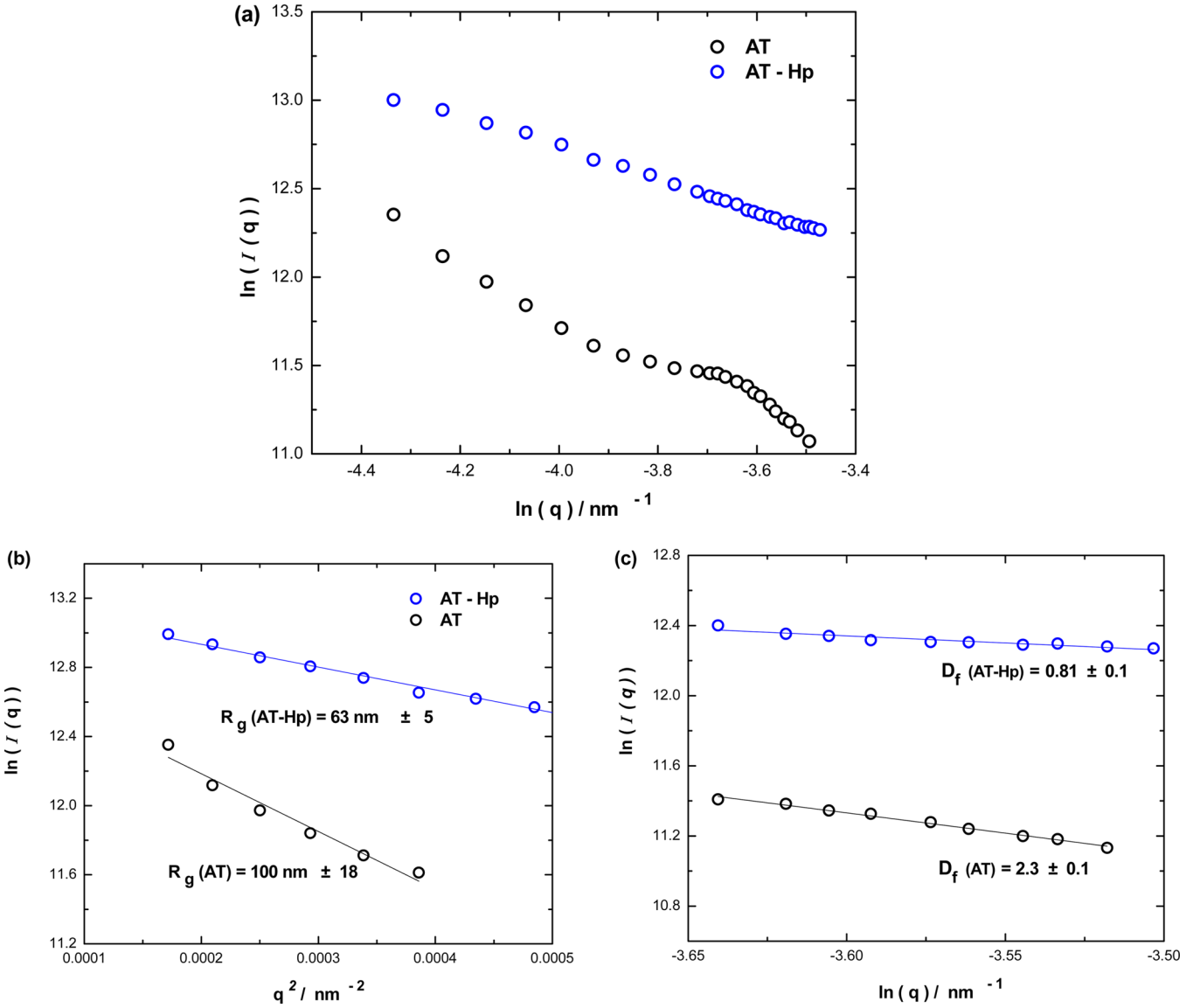

Figure 9. SLS of 1 g/L AT and 1 g/L AT and 0.1 g/L Hp (r = 0.1) in 10 mM NaCl, pH = 6.2: (a) Scattering intensity (I) as a function of scattering vector (q); (b) Guinier plot to determine R_g in the low-q region and (c) high-q region to determine fractal dimensions of AT aggregates and AT−Hp complex.

different path involving Hp diffusion onto and into aggregates, and a variety of subsequent kinetically controlled steps which cannot be readily identified by the current methods. The structure of the aggregate may play a role at least as significant as the intrinsic protein−Hp molecular affinity discussed above.

To support this latter hypothesis, fractal dimensions of AT aggregates were determined by static light scattering (Figure 9) and compared to published results for BSA. The difference between D_f(AT) = 2.3 ± 0.1 (Figure 9c) and 1.7 (BSA)[56] supports the argument that the greater density for AT aggregates makes them impervious to dissolution by Hp. However, when Hp is initially present with AT at pH 8 and r = 0.1 (prior to adjustment to pH 6.1), similar SLS measurements lead to D_f(AT−Hp) = 0.8 ± 0.1, consistent with a highly extended rodlike chain. Since AT is net-negative at this pH, both steric and electrostatic effects lead to intrapolymer repulsion in the Hp−AT complex and consequent chain stiffness. To our knowledge, this is the first reported measurement of the fractal dimension of an Hp−protein complex. Nominally, the values of R_g/R_h are 0.8 and 0.9 for aggregated AT and AT−Hp complex, respectivel,y from the Guinier plot shown in Figure 9b. The former, very close to the limiting value for spheres, is consistent with the large value of D_f, but the latter is not consistent with the extended conformation deduced from D_f = 0.8. These ratios must be considered in the light of the averaging of signals from large and small scatterers for both systems, unavoidable for SANS and arbitrary for DLS. These averages tend to be weighted more toward the smaller species in Malvern due to back-scattering. More accurate results will require angle dependence of diffusion coefficients complementary to Figure 9a.

CONCLUSIONS

Heparin (Hp) inhibits and reverses aggregation more completely for BSA than for antithrombin (AT). Since heparin binds more strongly to AT, this difference is not due to the conversion of protein monomer/dimer to nonaggregating complex, which would be greater for Hp. The reduced effects

dx.doi.org/10.1021/la4039232 | Langmuir 2014, 30, 278−287

of heparin for AT occur because the relatively low concentration of uncomplexed AT monomer aggregates far more extensively than the more abundant BSA monomer/dimer. The values of pH at which complexes are first observed at different ionic strengths, relative to pI—a measure of the ability of binding to overcome repulsion between heparin and global protein charge—is in good qualitative agreement with measurements of binding constants by FACCE. These two measures of protein−heparin affinity are shown to be consistent with protein charge anisotropy as revealed by electrostatic modeling. In contrast to inhibition, the reversal of protein aggregation by heparin is also influenced by aggregate structure: the low fractal dimensions of BSA aggregates make them more susceptible to dissolution mediated by heparin binding.

AUTHOR INFORMATION

Corresponding Author

*E-mail: dubin@chem.umass.edu.

Notes

The authors declare no competing financial interest.

ACKNOWLEDGMENTS

This work was supported by the National Science Foundation (CHE-0619039). B.Z. acknowledges a Bradspies Research Fellowship. We thank Erin Sutherland for the early method development in turbidimetric detection of time-dependent aggregation and GTC Biotherapeutics for providing ATyrn.

REFERENCES

(1) Suk, J. Y.; Zhang, F.; Balch, W. E.; Linhardt, R. J.; Kelly, J. W. Heparin Accelerates Gelsolin Amyloidogenesis†. *Biochemistry* **2006**, *45*, 2234−2242.

(2) Bravo, R.; Arimon, M.; Valle-Delgado, J. J.; García, R.; Durany, N.; Castel, S.; Cruz, M.; Ventura, S.; Fernàndez-Busquets, X. Sulfated Polysaccharides Promote the Assembly of Amyloid β1−42 Peptide into Stable Fibrils of Reduced Cytotoxicity. *J. Biol. Chem.* **2008**, *283*, 32471−32483.

(3) Nielsen, S. B.; Yde, P.; Giehm, L.; Sundbye, S.; Christiansen, G.; Mathiesen, J.; Jensen, M. H.; Jensen, P. H.; Otzen, D. E. Multiple Roles of Heparin in the Aggregation of p25α. *J. Mol. Biol.* **2012**, *421*, 601−615.

(4) Vieira, T. C.; Reynaldo, D. P.; Gomes, M. P.; Almeida, M. S.; Cordeiro, Y.; Silva, J. L. Heparin Binding by Murine Recombinant Prion Protein Leads to Transient Aggregation and Formation of RN-Resistant Species. *J. Am. Chem. Soc.* **2011**, *133*, 334−344.

(5) Silva, J. L.; Vieira, T. C.; Gomes, M. P.; Rangel, L. P.; Scapin, S. M.; Cordeiro, Y. Experimental Approaches to the Interaction of the Prion Protein with Nucleic Acids and Glycosaminoglycans: Modulators of the Pathogenic Conversion. *Methods* **2011**, *53*, 306−317.

(6) Zhu, H.; Yu, J.; Kindy, M. S. Inhibition of Amyloidosis Using Low-Molecular-Weight Heparins. *Mol. Med.* **2001**, *7*, 517−522.

(7) Wilhelmus, M. M.; de Waal, R. M.; Verbeek, M. M. Heat Shock Proteins and Amateur Chaperones in Amyloid-Beta Accumulation and Clearance in Alzheimer's Disease. *Mol. Neurobiol.* **2007**, *35*, 203−216.

(8) Vilasi, S.; Sarcina, R.; Maritato, R.; De Simone, A.; Irace, G.; Sirangelo, I. Heparin Induces Harmless Fibril Formation in Amyloidogenic W7FW14F Apomyoglobin and Amyloid Aggregation in Wild-Type Protein In Vitro. *PLoS ONE* **2011**, *6*.

(9) Bergamaschini, L.; Rossi, E.; Vergani, C.; De Simoni, M. G. Alzheimer's Disease: Another Target for Heparin Therapy. *Sci. World J.* **2009**, *9*, 891−908.

(10) Miura, Y.; Yasuda, K.; Yamamoto, K.; Koike, M.; Nishida, Y.; Kobayashi, K. Inhibition of Alzheimer Amyloid Aggregation with Sulfated Glycopolymers. *Biomacromolecules* **2007**, *8*, 2129−2134.

(11) Calamai, M.; Chiti, F.; Dobson, C. M. Amyloid Fibril Formation Can Proceed from Different Conformations of a Partially Unfolded Protein. *Biophys. J.* **2005**, *89*, 4201−4210.

(12) Carrotta, R.; Manno, M.; Bulone, D.; Martorana, V.; Biagio, P. L. S. Protofibril Formation of Amyloid β-Protein at Low pH via a Noncooperative Elongation Mechanism. *J. Biol. Chem.* **2005**, *280*, 30001−30008.

(13) Jain, S.; Udgaonkar, J. B. Defining the Pathway of Wormlike Amyloid Fibril Formation by the Mouse Prion Protein by Delineation of the Productive and Unproductive Oligomerization Reactions. *Biochemistry* **2011**, *50*, 1153−1161.

(14) Park, S.; Saven, J. G. Simulation of pH-Dependent Edge Strand Rearrangement in Human Beta-2-microglobulin. *Protein Sci.* **2006**, *15*, 200−207.

(15) Chiti, F.; Bucciantini, M.; Capanni, C.; Taddei, N.; Dobson, C. M.; Stefani, M. Solution Conditions Can Promote Formation of Either Amyloid Protofilaments or Mature Fibrils from the HypF N-Terminal Domain. *Protein Sci.* **2001**, *10*, 2541−2547.

(16) Chiti, F.; Dobson, C. M. Amyloid Formation by Globular Proteins under Native Conditions. *Nat. Chem. Biol.* **2009**, *5*, 15−22.

(17) Wang, G.; Johnson, A. J.; Kaltashov, I. A. Evaluation of Electrospray Ionization Mass Spectrometry as a Tool for Characterization of Small Soluble Protein Aggregates. *Anal. Chem.* **2011**, *84*, 1718−1724.

(18) Zhou, A.; Carrell, R. W. Dimers Initiate and Propagate Serine Protease Inhibitor Polymerisation. *J. Mol. Biol.* **2008**, *375*, 36−42.

(19) Vetri, V.; Librizzi, F.; Leone, M.; Militello, V. Thermal Aggregation of Bovine Serum Albumin at Different pH: Comparison with Human Serum Albumin. *Eur. Biophys. J.* **2007**, *36*, 717−725.

(20) Holm, N. K.; Jespersen, S. K.; Thomassen, L. V.; Wolff, T. Y.; Sehgal, P.; Thomsen, L. A.; Christiansen, G.; Andersen, C. B.; Knudsen, A. D.; Otzen, D. E. Aggregation and Fibrillation of Bovine Serum Albumin. *Biochim. Biophys. Acta, Proteins Proteomics* **2007**, *1774*, 1128−1138.

(21) Militello, V.; Casarino, C.; Emanuele, A.; Giostra, A.; Pullara, F.; Leone, M. Aggregation Kinetics of Bovine Serum Albumin Studied by FTIR Spectroscopy and Light Scattering. *Biophys. Chem.* **2004**, *107*, 175−187.

(22) Xu, Y.; Seeman, D.; Yan, Y.; Sun, L.; Post, J.; Dubin, P. L. Effect of Heparin on Protein Aggregation: Inhibition versus Promotion. *Biomacromolecules* **2012**, *13*, 1642−1651.

(23) Schreiber, G.; Haran, G.; Zhou, H. X. Fundamental Aspects of Protein−Protein Association Kinetics. *Chem. Rev.* **2009**, *109*, 839−860.

(24) Vijayakumar, M.; Wong, K. Y.; Schreiber, G.; Fersht, A. R.; Szabo, A.; Zhou, H. X. Electrostatic Enhancement of Diffusion-Controlled Protein−Protein Association: Comparison of Theory and Experiment on Barnase and Barstar. *J. Mol. Biol.* **1998**, *278*, 1015−1024.

(25) Giger, K.; Vanam, R. P.; Seyrek, E.; Dubin, P. L. Suppression of Insulin Aggregation by Heparin. *Biomacromolecules* **2008**, *9*, 2338−2344.

(26) Meakin, P. A Historical Introduction to Computer Models for Fractal Aggregates. *J. Sol-Gel Sci. Technol.* **1999**, *15*, 97−117.

(27) Kayitmazer, A. B.; Quinn, B.; Kimura, K.; Ryan, G. L.; Tate, A. J.; Pink, D. A.; Dubin, P. L. Protein Specificity of Charged Sequences in Polyanions and Heparins. *Biomacromolecules* **2010**, *11*, 3325−3331.

(28) Bourgault, S.; Solomon, J. P.; Reixach, N. l.; Kelly, J. W. Sulfated Glycosaminoglycans Accelerate Transthyretin Amyloidogenesis by Quaternary Structural Conversion. *Biochemistry* **2010**, *50*, 1001−1015.

(29) Kayitmazer, A. B.; Seeman, D.; Minsky, B. B.; Dubin, P. L.; Xu, Y. Protein−Polyelectrolyte Interactions. *Soft Matter* **2013**, *9*, 2553−2583.

(30) Jones, L. S.; Yazzie, B.; Middaugh, C. R. Polyanions and the Proteome. *Mol. Cell. Proteomics* **2004**, *3*, 746−769.

(31) Record, M. T., Jr.; Lohman, M. L.; De Haseth, P. Ion Effects on Ligand−Nucleic Acid Interactions. *J. Mol. Biol.* **1976**, *107*, 145−158.

(32) Mascotti, D. P.; Lohman, T. M. Thermodynamic Extent of Counterion Release upon Binding Oligolysines to Single-Stranded Nucleic Acids. *Proc. Natl. Acad. Sci. U.S.A.* **1990**, *87*, 3142−3146.
(33) Fenley, M. O.; Russo, C.; Manning, G. S. Theoretical Assessment of the Oligolysine Model for Ionic Interactions in Protein−DNA Complexes. *J. Phys. Chem. B* **2011**, *115*, 9864−9872.
(34) Mascotti, D. P.; Lohman, T. M. Thermodynamics of Charged Oligopeptide−Heparin Interactions. *Biochemistry* **1995**, *34*, 2908−2915.
(35) Grymonpre, K. R.; Staggemeier, B. A.; Dubin, P. L.; Mattison, K. W. Identification by Integrated Computer Modeling and Light Scattering Studies of an Electrostatic Serum Albumin−Hyaluronic Acid Binding Site. *Biomacromolecules* **2001**, *2*, 422−429.
(36) Seyrek, E.; Dubin, P. L.; Tribet, C.; Gamble, E. A. Ionic Strength Dependence of Protein−Polyelectrolyte Interactions. *Biomacromolecules* **2003**, *4*, 273−282.
(37) Seyrek, E.; Dubin, P. L.; Henriksen, J. Nonspecific Electrostatic Binding Characteristics of the Heparin−Antithrombin Interaction. *Biopolymers* **2007**, *86*, 249−259.
(38) Zhang, C.; Lillie, R.; Cotter, J.; Vaughan, D. Lysozyme Purification from Tobacco Extract by Polyelectrolyte Precipitation. *J. Chromatogr. A* **2005**, *1069*, 107−112.
(39) Peram, T.; McDonald, P.; Carter-Franklin, J.; Fahrner, R. Monoclonal Antibody Purification Using Cationic Polyelectrolytes: An Alternative to Column Chromatography. *Biotechnol. Prog.* **2010**, *26*, 1322−1331.
(40) Zhao, J. Y.; Ford, C. F.; Glatz, C. E.; Rougvie, M. A.; Gendel, S. M. Polyelectrolyte Precipitation of Beta-Galactosidase Fusions Containing Poly-Aspartic Acid Tails. *J. Biotechnol.* **1990**, *14*, 273−283.
(41) Levi, V.; González Flecha, F. L. Reversible Fast-Dimerization of Bovine Serum Albumin Detected by Fluorescence Resonance Energy Transfer. *Biochim. Biophys. Acta, Proteins Proteomics* **2002**, *1599*, 141−148.
(42) Rocchia, W.; Alexov, E.; Honig, B. Extending the Applicability of the Nonlinear Poisson−Boltzmann Equation: Multiple Dielectric Constants and Multivalent Ions†. *J. Phys. Chem. B* **2001**, *105*, 6507−6514.
(43) Rocchia, W.; Sridharan, S.; Nicholls, A.; Alexov, E.; Chiabrera, A.; Honig, B. Rapid Grid-Based Construction of the Molecular Surface and the Use of Induced Surface Charge to Calculate Reaction Field Energies: Applications to the Molecular Systems and Geometric Objects. *J. Comput. Chem.* **2002**, *23*, 128−137.
(44) Tanford, C.; Kirkwood, J. G. Theory of Protein Titration Curves. I. General Equations for Impenetrable Spheres. *J. Am. Chem. Soc.* **1957**, *79*, 5333−5339.
(45) Xu, Y.; Yan, Y.; Seeman, D.; Sun, L.; Dubin, P. L. Multimerization and Aggregation of Native-State Insulin: Effect of Zinc. *Langmuir* **2012**, *28*, 579−586.
(46) Yan, Y.; Seeman, D.; Zheng, B.; Kizilay, E.; Xu, Y.; Dubin, P. L. pH-Dependent Aggregation and Disaggregation of Native Beta-Lactoglobulin in Low Salt. *Langmuir* **2013**, *29*, 4584−4593.
(47) Majhi, P. R.; Ganta, R. R.; Vanam, R. P.; Seyrek, E.; Giger, K.; Dubin, P. L. Electrostatically Driven Protein Aggregation: Beta-Lactoglobulin at Low Ionic Strength. *Langmuir* **2006**, *22*, 9150−9159.
(48) Barbosa, L. R.; Ortore, M. G.; Spinozzi, F.; Mariani, P.; Bernstorff, S.; Itri, R. The Importance of Protein−Protein Interactions on the pH-Induced Conformational Changes of Bovine Serum Albumin: A Small-Angle X-ray Scattering Study. *Biophys. J.* **2010**, *98*, 147−157.
(49) El Kadi, N.; Taulier, N.; Le Huerou, J. Y.; Gindre, M.; Urbach, W.; Nwigwe, I.; Kahn, P. C.; Waks, M. Unfolding and Refolding of Bovine Serum Albumin at Acid pH: Ultrasound and Structural Studies. *Biophys. J.* **2006**, *91*, 3397−3404.
(50) Estey, T.; Kang, J.; Schwendeman, S. P.; Carpenter, J. F. BSA Degradation under Acidic Conditions: A Model for Protein Instability during Release from PLGA Delivery Systems. *J. Pharm. Sci.* **2006**, *95*, 1626−1639.
(51) Zhou, A.; Stein, P. E.; Huntington, J. A.; Carrell, R. W. Serpin Polymerization Is Prevented by a Hydrogen Bond Network That Is Centered on His-334 and Stabilized by Glycerol. *J. Biol. Chem.* **2003**, *278*, 15116−15122.
(52) Wang, K.; Kurganov, B. I. Kinetics of Heat- and Acidification-Induced Aggregation of Firefly Luciferase. *Biophys. Chem.* **2003**, *106*, 97−109.
(53) Kurganov, B. I. Kinetics of Protein Aggregation. Quantitative Estimation of the Chaperone-Like Activity in Test-Systems Based on Suppression of Protein Aggregation. *Biochemistry (Moscow)* **2002**, *67*, 409−422.
(54) Olson, S. T.; Bjork, I.; Sheffer, R.; Craig, P. A.; Shore, J. D.; Choay, J. Role of the Antithrombin-Binding Pentasaccharide in Heparin Acceleration of Antithrombin−Proteinase Reactions. Resolution of the Antithrombin Conformational Change Contribution to Heparin Rate Enhancement. *J. Biol. Chem.* **1992**, *267*, 12528−12538.
(55) Jho, Y. S.; Safran, S. A.; In, M.; Pincus, P. A. Effect of Charge Inhomogeneity and Mobility on Colloid Aggregation. *Langmuir* **2012**, *28*, 8329−8336.
(56) Magazu, S.; Maisano, G.; Mallamace, F.; Micali, N. Growth of Fractal Aggregates in Water Solutions of Macromolecules by Light Scattering. *Phys. Rev. A* **1989**, *39*, 4195−4200.